

1
2
3
4
5
6
7
8
9
10
11
12
13
14
15
16
17
18
19
20
21
22
23
24

Restoring vascular endothelial autophagic flux reduces atherosclerotic lesions

Shruti Chatterjee¹, Marouane Kheloufi¹, Stephane Mazlan¹, Xavier Loyer¹, Timothy A. McKinsey², Pierre-Michaël Coly^{1#}, Chantal M. Boulanger^{1#}

¹ Université de Paris, PARCC, INSERM, F-75015 Paris

² Department of Medicine, Division of Cardiology and Consortium for Fibrosis Research & Translation, University of Colorado Anschutz Medical Campus, Aurora, CO, USA

These authors contributed equally to this work.

Running title: Endothelial autophagic flux activation hampers inflammation

Corresponding author:

Chantal M. Boulanger, PhD, Inserm UMR 970, Paris Cardiovascular Research Center,
56 Rue Leblanc, F-75015 Paris -- Tel +33153988086; chantal.boulanger@inserm.fr

Abstract word count: 259

Manuscript word count: 6158

Figures: 8

Supplementary figures: 7

Supplementary tables: 3

25 **Abstract:**

26 Atherosclerotic lesions preferentially develop in arterial areas exposed to low shear stress, where
27 endothelial cells express a pro-inflammatory, apoptotic, and senescent phenotype. Autophagy is
28 a lysosomal mechanism that recycles damaged organelles and protein aggregates to maintain
29 cellular homeostasis. Stimulation of autophagy in high shear stress conditions is an
30 atheroprotective process. Conversely, endothelial cells exposed to atheroprone low shear stress
31 present a defective autophagic flux, which favors a pro-inflammatory phenotype and the
32 formation of atherosclerotic lesions. Since an efficient autophagic flux is dependent on α -tubulin
33 acetylation, which is reduced under low shear stress, we hypothesized that increasing α -tubulin
34 acetylation could restore adequate levels of autophagy in endothelial cells exposed to low shear
35 stress. We found that blocking Histone Deacetylase 6 (HDAC6) activity, either by
36 pharmacological inhibition (Tubastatin-A) or genetic approaches (shHDAC6), raised levels of
37 acetylated α -tubulin, as well as LC3-II/I ratio, LC3 punctae area and autophagic flux in cultured
38 endothelial cells exposed to low shear stress. This effect was associated with a reduced
39 expression of inflammatory markers (Intercellular adhesion molecule-1 (ICAM-1), Vascular cell
40 Adhesion Protein-1 (VCAM-1) and Monocyte Chemoattractant Protein-1 (MCP-1)) in Tumor
41 Necrosis Factor-alpha (TNF- α)-stimulated cells. We observed increased endothelial autophagic
42 flux in the aortic arch of the *HDAC6^{-/-}/ApoE^{-/-}* mice. Subsequently, atherosclerotic plaque size
43 was significantly reduced in the atheroprone areas of chimeric *HDAC6^{-/-}/ApoE^{-/-}* mice,
44 transplanted with *HDAC6^{+/+}/ApoE^{-/-}* bone marrow, when compared to *HDAC6^{+/+}/ApoE^{-/-}*
45 littermate controls. Taken together, these results indicate that targeting α -tubulin acetylation, via
46 HDAC6-inhibition, may be an interesting strategy to restore endothelial autophagic flux and to
47 promote an atheroprotective endothelial phenotype despite unfavorable shear stress conditions.

48
49 **Keywords:** Endothelial cells, Autophagy, Atherosclerosis, HDAC6, Tubastatin-A, inflammation,
50 ICAM-1, VCAM-1, MCP-1

51
52 **Abbreviations:** CQ: Chloroquine; ICAM-1: Intercellular adhesion molecule 1; HDAC6: Histone
53 Deacetylase 6; HUVEC: Human umbilical vein endothelial cell; LC3: microtubule-associated
54 protein 1 light chain 3 β ; MCP-1: Monocyte chemoattractant protein 1; SS: Shear stress; TNF- α :
55 Tumor necrosis factor alpha; TUBA: Tubastatin-A; VCAM-1: Vascular cell adhesion protein 1

56
57
58

59 **Introduction**

60 Over the years, several studies have shown that atherosclerotic plaques form in predisposed areas
61 such as arterial bifurcations, or the inner curvature of aortic bends. In these regions, endothelial
62 cells are exposed to disturbed blood flow, which exerts low levels of shear stress (SS) on the
63 vessel wall (Souilhol et al. 2020; Lee and Chiu 2019; Baeyens et al. 2016). Conversely, cells
64 exposed to laminar flow, which generates high SS, exhibit an anti-inflammatory, anti-senescent
65 and anti-apoptotic phenotype, resulting in reduced plaque formation. Low SS triggers the
66 expression of various inflammatory markers, such as adhesion proteins and chemokines (Chiu
67 and Chien 2011; Souilhol et al. 2020). This in turn favors the recruitment of leukocytes to the
68 lesion site and contributes to the initial stages of plaque formation. While the mechanisms by
69 which SS regulates the endothelial phenotype have yet to be fully elucidated, our group has
70 previously demonstrated that a modulation of endothelial macroautophagy (hereafter referred to
71 as autophagy) is a determining factor (Vion et al. 2017).

72

73 Autophagy is an evolutionarily conserved, cytoprotective mechanism, which helps degrade and
74 recycle damaged organelles and proteins, to maintain cellular homeostasis (Feng et al. 2014). As
75 such, autophagy occurs at a basal rate under physiological conditions, and is amplified under
76 stress conditions, such as nutrient starvation, to promote cell survival (Wen and Klionsky 2016).
77 Defects in the autophagic process have been reported in multiple pathologies, including cancer,
78 neurodegenerative, auto-immune and cardiovascular diseases (Mizushima et al. 2008;
79 Mizushima 2018; Levy, Towers, and Thorburn 2017; Mialet-Perez and Vindis 2017). Often, the
80 defect lies in the crucial autolysosome formation step, wherein autophagosomes fuse with
81 lysosomes to allow the degradation of their content (Levy, Towers, and Thorburn 2017; Wong,
82 Cheung, and Ip 2011). Low SS has been shown to inhibit autophagic flux in endothelial cells,
83 which then contributes to the onset of a pro-inflammatory and senescent phenotype (Guo et al.
84 2017; Chiu et al. 2004; Vion et al. 2017).

85

86 While numerous factors can regulate autophagy, studies have highlighted the importance of
87 several post-translational tubulin modifications and their effects on microtubule dynamics and
88 cellular trafficking (Mackeh et al. 2013). In addition to concentrating signaling pathways that
89 stimulate autophagosome formation, microtubules are integral to the movement of pre-
90 autophagosomal structures, as well as the transport of mature autophagosomes towards
91 lysosomes (Mackeh et al. 2013; Ravikumar et al. 2005; Xie et al. 2010). In that sense,
92 microtubules stabilized through α -tubulin acetylation favor the recruitment and walking of motor

93 proteins, resulting in enhanced cellular trafficking (Xie et al. 2010). Interestingly, endothelial
94 cells exposed to high SS have been shown to express elevated levels of acetylated α -tubulin
95 when compared to cells cultured under static conditions (McCue et al. 2006). This may, in part,
96 explain why endothelial cells exposed to high SS have an increased autophagic activity. The
97 level of endothelial α -tubulin acetylation is regulated by the cytosolic protein deacetylase
98 Histone Deacetylase 6 (HDAC6) (Birdsey et al. 2012; Eshun-Wilson et al. 2019). The
99 phosphorylated active form of HDAC6 in particular, is known to remain active mainly in the
100 cytosol (Ustinova et al. 2020; S. Chen et al. 2010).

101 Based on these data, we hypothesized that increasing α -tubulin acetylation, through HDAC6
102 inhibition, could restore adequate levels of autophagy in endothelial cells exposed to atheroprone
103 low SS. In this study, we found that targeting HDAC6 with a selective inhibitor, Tubastatin-A, or
104 an shRNA, led to hyperacetylation of α -tubulin in HUVECs exposed to low SS. This then
105 resulted in an increased autophagic flux and reduced expression of inflammatory markers
106 ICAM-1, VCAM-1 and MCP-1. *In vivo* experiments demonstrated that knocking out *HDAC6* in
107 hypercholesteremic mice reduces the formation of atherosclerotic lesions in otherwise
108 predisposed areas in the aorta.

109

110

111 **Results**

112 **Shear stress regulates levels of acetylated α -tubulin in endothelial cells.** As previously
113 described by McCue *et.al*, shear stress regulates elongation and polarity of endothelial cells via
114 reorganization of the cytoskeleton (McCue et al. 2006). Therefore, we first sought to verify if
115 this was also the case in our experimental model, by measuring acetylated α -tubulin expression
116 in low passage cultured HUVECs exposed to either physiological high or low SS. Western blot
117 data indicated higher levels of acetylated α -tubulin in HUVECs exposed to high SS for 24 hours,
118 when compared to HUVECs exposed to low SS (Suppl. Fig. 1).

119

120 **HDAC6 activity is increased in endothelial cells exposed to low SS.** α -tubulin modifications
121 result from the balance between acetyltransferases and deacetylases such as HDAC6. We
122 hypothesized that the effects of shear stress on levels of acetylated α -tubulin could be relayed by
123 a modulation of HDAC6 activity. Previous data indicated that HDAC6 interacts with α -tubulin
124 when it is phosphorylated at Ser22 by GSK-3 β (S. Chen et al. 2010). The expression and
125 localization of both the canonical and phosphorylated forms of HDAC6 were analyzed by
126 immunofluorescence (Fig.1A). While no difference in the staining intensity of total-HDAC6 was
127 observed, we found that HUVECs exposed to low SS exhibited higher levels of phosphorylated-
128 HDAC6, compared to cells exposed to high SS conditions (Fig.1B). Furthermore, using a
129 fluorometric assay (Lemon et al. 2011), we found that HDAC6 activity was significantly higher
130 in cells exposed to low SS, when compared to high SS (Fig. 1C). Taken all together, these results
131 indicate that endothelial cells exposed to atheroprone low SS have a higher HDAC6 activity than
132 cells exposed to atheroprotective high SS.

133

134 **HDAC6 inhibition increases levels of acetylated α -tubulin.** To evaluate the consequences of
135 inhibiting HDAC6 activity in endothelial cells, we chose to utilize a known HDAC6 inhibitor,
136 Tubastatin-A (Butler et al. 2010). HUVECs were exposed to low SS for 24h, under Tubastatin-A
137 treatment (3 μ M) or vehicle (DMSO). Acetylated α -tubulin expression levels were measured by
138 Western blot and normalized to GAPDH and total α -tubulin. As expected, Tubastatin-A
139 treatment markedly increased levels of acetylated α -tubulin in HUVECs exposed to low SS
140 (Suppl. Fig. 2A and 2B). We further characterized the effects of Tubastatin-A on acetylated α -
141 tubulin by immunofluorescence staining. In accordance with our Western blot data, we found
142 that cells treated with Tubastatin-A presented a more intense acetylated α -tubulin signal.
143 Additionally, we observed that acetylated α -tubulin displayed a more organized pattern in

144 Tubastatin-A-treated cells (Suppl. Fig. 2C and 2D). This indicates that inhibition of HDAC6
145 leads to stabilization of a polymerized α -tubulin network.

146

147 **HDAC6 inhibition restores autophagic activity in endothelial cells exposed to low SS.** As
148 previously described by Mackeh et al. (Mackeh et al. 2013) stable acetylated microtubules are
149 required for the efficient formation of autophagosomes, as well as for their fusion with
150 lysosomes. This prompted us to evaluate whether blocking α -tubulin deacetylation, via HDAC6
151 inhibition, would stimulate autophagic activity in cells exposed to low SS. We first assessed
152 autophagic activity by measuring LC3-II/I ratio in HUVECs. In accordance with our previous
153 findings, cells exposed to low SS for 24h displayed a lower LC3-II/I ratio than cells exposed
154 high SS (Fig.2). Treatment with Tubastatin-A, in low SS conditions, led to an elevation of the
155 LC3-II/I ratio to approximately twice that of control conditions (Fig. 2A and 2B). Similar results
156 were obtained when expressing LC3 as a ratio of LC3-II to GAPDH. Interestingly, treating cells
157 with Tubastatin-A did not modify levels of other essential autophagy proteins, such as ATG5
158 (Suppl. Fig. 3A and 3B) and p62 (Suppl. Fig. 3C and 3D). We obtained comparable data when
159 measuring the area of LC3-positive puncta per cell by immunostaining. LC3 staining was
160 consistently less abundant in HUVECs exposed to low SS. However, treating cells with
161 Tubastatin-A elevated the area of LC3-positive structures per cell to levels (Fig. 2C and 2D).

162 To confirm that HDAC6 inhibition led to autophagy stimulation, we used a tandem LC3-B
163 fluorescently tagged with mRFP and GFP. In this assay, autophagosomes emit a yellow signal
164 (mRFP-GFP-LC3), and their maturation into autolysosomes is attested by a red signal due to
165 quenching of the GFP fluorescence in low pH environments (Fig. 3A). We therefore evaluated
166 autophagic flux by quantifying the ratio of autolysosomes/autophagosomes per cell (Fig. 3B). As
167 previously demonstrated, HUVECs exposed to high SS conditions had approximately twice the
168 number of autolysosomes than those exposed to low SS conditions, while the number of
169 autophagosomes remained similar (Fig. 3C and 3D). This indicated that maturation of
170 autophagosomes into autolysosomes was impaired under low SS conditions. Treatment with
171 Rapamycin (1 μ M), a known autophagy inducer, resulted in a slight decrease in the number of
172 autophagosomes, and an increase in the number of autolysosomes. A similar trend was observed
173 in HUVECs treated with Tubastatin-A under low SS conditions, suggesting that HDAC6
174 inhibition stimulates autophagic flux in endothelial cells exposed to low SS. However, these
175 results could also be explained by an increase in autophagosome biogenesis. To test this
176 hypothesis, we examined the effects of Tubastatin-A in combination with chloroquine, a
177 lysosomotropic agent that neutralizes the acidic pH of lysosomes, thereby blocking the fusion

178 between autophagosomes and lysosomes (Mauthe et al. 2018). As expected, treating cells with
179 chloroquine (300 μ M) resulted in an increase in the number of autophagosomes (Fig. 3E and 3F).
180 In the presence of chloroquine, Tubastatin-A failed to elevate the number of autolysosomes, but
181 increased the number of autophagosomes, which suggests an acceleration of autophagosome
182 formation (Fig. 3G). Taken together these data indicate that HDAC6 inhibition may stimulate
183 autophagic flux, by increasing autophagosome biogenesis and maturation, in endothelial cells
184 exposed to low SS.

185

186 **HDAC6 inhibition reduces the endothelial inflammation caused by exposure to low SS**
187 **conditions.** Our group has previously demonstrated that the defect in endothelial autophagy,
188 which occurs in low SS areas, causes inflammation and favors the development of
189 atherosclerotic lesions (Vion et al. 2017). Since Tubastatin-A treatment restored autophagic flux
190 in endothelial cells, we wondered if this would also hamper the pro-inflammatory consequences
191 of exposure to low SS conditions. To induce inflammation, cells were treated with TNF- α , at
192 1ng/mL, for the last 12 hours of the shear stress experiment. By western blot, we assessed the
193 expression levels of inflammatory markers ICAM-1 and VCAM-1. Firstly, a pronounced
194 elevation of ICAM-1 (Fig. 4A and 4C) and VCAM-1 (Fig. 4B and 4D) expression was observed
195 in response to TNF- α treatment. HUVECs exposed to low SS expressed higher levels of both
196 proteins, as compared to cells exposed to high SS. However, treating cells with Tubastatin-A
197 significantly reduced levels of ICAM-1 and VCAM-1 in cells exposed to low SS. Interestingly,
198 Tubastatin-A also suppressed the TNF- α -induced elevation in phospho-NF- κ B levels (Suppl.
199 Fig. 4). We next measured the concentration of MCP-1 found in the HUVEC supernatant, by
200 ELISA. We found that cells exposed to low SS released approximately 5 times more MCP-1
201 than cells exposed to high SS conditions. Here also, adding Tubastatin-A to cells, markedly
202 reduced levels of MCP-1 released by cells exposed to low SS (Fig. 4E). These results show that
203 HDAC6 inhibition hampers low SS-induced endothelial inflammation.

204 To confirm these data, we knocked down HDAC6 in HUVECs using a shRNA-carrying
205 lentivirus. With this strategy, we observed a 30% reduction in the expression of HDAC6 (Fig.
206 5A and 5B). This was sufficient to increase levels of acetylated α -tubulin by 50% (Fig. 5C).
207 HDAC6-knockdown also led to an increase in the LC3-II/I ratio (Fig. 5D), while reducing
208 ICAM-1 (Fig. 5E) and VCAM-1 (Fig. 5F) expression as well as MCP-1 release (Fig. 5G) in
209 TNF α -treated cells. Taken together, these data show that blocking HDAC6, by a
210 pharmacological or a genetic approach, increases the level of acetylated α -tubulin, restores
211 endothelial autophagy, and reduces endothelial inflammation in cells exposed to low SS.

212

213 **The anti-inflammatory effects of HDAC6 inhibition are relayed by autophagy.** To verify
214 whether the anti-inflammatory effects of HDAC6-inhibition were linked to a restored autophagic
215 flux, we assessed the effects of Tubastatin-A in cells deficient for autophagosome formation (i.e.,
216 HUVECs infected with a lentivirus carrying an ATG5 shRNA). Knocking down ATG5 has
217 indeed been shown to reduce autophagosome biogenesis. As expected, this approach resulted in
218 lowered ATG5 protein levels (Fig. 6A) and LC3-II/I ratio (Fig. 6B). We verified that the
219 HDAC6 protein was still present under shATG5 conditions (Suppl. Fig. 6A and 6B), and that
220 Tubastatin-A was able to substantially increase levels of acetylated α -tubulin (Suppl. Fig. 6A and
221 6C). In these ATG5-deficient endothelial cells, the anti-inflammatory effect of Tubastatin-A
222 treatment was significantly reduced, as indicated by the lower expression of ICAM-1 (Fig. 6C
223 and Suppl. Fig. 5A), VCAM-1 (Fig. 6D and Suppl. Fig. 5B) and the impaired MCP-1 release
224 (Fig. 6E and Suppl. Fig. 5C). These data suggest that the anti-inflammatory effects of HDAC6-
225 inhibition rely on a functional autophagic activity.

226

227 **Deletion of HDAC6 enhances autophagic flux in murine aortic arch.** To observe the effect of
228 HDAC6 deletion on autophagic activity *in vivo*, we performed *en face* staining of murine aorta
229 for LC3 in HDAC6^{-/-} / ApoE^{-/-} and littermate controls (HDAC6^{+/+} / ApoE^{-/-}). As expected, we
230 observed higher LC3 staining in high SS regions such the descending aorta, when compared to
231 the low SS region that is the aortic arch (Fig. 7A and 7B). Interestingly, LC3 staining was higher
232 in the arch of HDAC6^{-/-} animals compared to HDAC6^{+/+} controls (Fig. 7A and 7B). Following
233 this, we evaluated autophagic flux by measuring the colocalization of the LC3 with the
234 lysosomal marker LAMP2A. Similarly, colocalization of LC3 and LAMP2A was significantly
235 higher in the aortic arch of HDAC6^{-/-} animals compared to HDAC6^{+/+}, which led us to infer that
236 the absence of HDAC6 may favor promotion of autophagic flux in endothelial cells (Fig. 7C and
237 7D).

238

239 **Deletion of HDAC6 reduces atherosclerotic lesions in hypercholesterolemic mice.** To
240 evaluate the effect of HDAC6 deletion on atherosclerotic plaque development, chimeric HDAC6^{-/-}
241 / ApoE^{-/-} and their littermate controls (HDAC6^{+/+} / ApoE^{-/-}) mice were transplanted with
242 HDAC6^{+/+} / ApoE^{-/-} bone marrow and fed a high fat diet for 10 weeks. This regimen resulted in a
243 doubling of plasma cholesterol levels (Suppl. Fig. 7A). HDAC6 knockout had no effect on
244 cholesterol levels (Suppl. Fig. 7A), body and organ weight, nor did it alter cell count for different
245 populations in the blood (Suppl. Fig. 7B), or the immune cell profile in the spleen (Suppl. Fig.

246 7C) and bone marrow (Suppl. Fig. 7D). As previously, described, atherosclerotic plaques
247 preferentially formed low SS areas such as the inner curvature of the aortic arch and around
248 carotids, whereas high SS areas, such as the descending aorta, remained relatively protected (Fig.
249 8A). We found that plaque size was reduced by approximately 30% in the aortic arch of *HDAC6*-
250 knockout animals when compared to littermate controls (Fig.8B). Altogether, these results
251 demonstrate that HDAC6 inhibition stimulates autophagic flux, reduces inflammation, and limits
252 the development of atherosclerotic lesions in atheroprone low SS conditions.
253

254 **DISCUSSION**

255 Defect in endothelial autophagy occurs in low SS areas of the vasculature, therefore
256 favoring inflammation and the development of atherosclerotic lesions (Vion et al. 2017). Data
257 presented in this study show that increasing α -tubulin acetylation, via HDAC6 inhibition, can
258 restore adequate levels of endothelial autophagic flux, thereby reducing inflammation and plaque
259 development.

260 Shear stress influences the endothelial cell's ability to polarize and align, by
261 redistribution of the microtubule network and reorganization of the microtubule organizing
262 center (McCue et al. 2006). Microtubule stability can be attributed to several types of post-
263 translational modifications, such as acetylation, which are regulated by shear stress (Bailey et al.
264 2017; McCue et al. 2006). In line with these previous studies, we found that α -tubulin acetylation
265 on lysine 40 is increased in endothelial cells exposed to high SS. HDAC6 inhibition and
266 knockdown, significantly increased α -tubulin acetylation in HUVECs. HDAC6 phosphorylation
267 and activity was higher in cells exposed to atheroprone low SS when compared to cells exposed
268 to high SS. This difference may, in part, explain the higher microtubule stability observed in
269 atheroprotective SS conditions. Interestingly other pro-atherogenic stimuli, such as cigarette
270 smoke, were also found to increase HDAC6-phosphorylation (Borgas et al. 2016). At this point,
271 little is known about the regulation of HDAC6 by shear stress. Several upstream effectors have
272 been identified, however. HDAC6 can be phosphorylated by different kinases, including
273 glycogen synthetase kinase 3 β) (GSK-3 β). Studies performed in HUVECs have demonstrated
274 flow-induced activation of GSK-3 β through a $G\alpha_{q/11}$ -Akt-1-dependent pathway (McCue et al.
275 2006). Moreover, HDAC6 activation may also be relayed through the zeta isoform of Protein
276 Kinase C, which has been shown to be activated by oscillatory shear stress (Du et al. 2015). In
277 addition to post-translational modifications, recent work by Manea et al. has revealed that
278 multiple HDACs, including HDAC6, are upregulated in human carotid-derived atherosclerotic
279 lesions and in atherosclerotic aortas of *ApoE*^{-/-} mice (Manea et al. 2020). More data would be
280 needed to fully understand how different shear stress intensities modulate these pathways.

281 Tubastatin-A has a higher specificity for HDAC6, compared to other members of the
282 HDAC family (Butler et al. 2010). We found that Tubastatin-A treatment had a marked effect on
283 α -tubulin acetylation, and restored autophagic flux in HUVECs cultured in low SS conditions.
284 Similarly, we observed a greater colocalization of LC3 and the lysosomal marker LAMP-2, in the
285 aortic arch of *HDAC6*-knockout mice, indicating a more robust autophagic flux in endothelial
286 cells lacking HDAC6 and exposed to low SS. Interestingly, removing HDAC6 resulted in aortic
287 arch endothelial cells displaying similar autophagic flux levels to those observed in high SS

288 areas. Furthermore, our *in vitro* experiments performed in the presence of chloroquine revealed
289 that HDAC6 inhibition also increased the rate of autophagosome biogenesis, without modifying
290 the expression levels of essential autophagy proteins such as ATG5. While we cannot exclude
291 that other mechanisms may be relaying the effects of HDAC6-inhibition, we suspect that they
292 are mediated by increased trafficking of autophagic structures along acetylated microtubules.
293 Hyperacetylation of tubulin enhances the recruitment of motor proteins to microtubules, which
294 subsequently contribute to the concentration of signaling pathways involved in autophagosome
295 biogenesis and to the transport of mature autophagosomes towards lysosomes (Geeraert et al.
296 2010; Bánréti, Sass, and Graba 2013). Several studies have indeed described impaired
297 autophagosome and autolysosome formation in conditions where microtubules were
298 disassembled using taxol or nocadazol (Geeraert et al. 2010; Köchl et al. 2006; Xie et al. 2010).
299 More recently, Majora et al. demonstrated that Tubastatin-A and the pan-HDAC inhibitor,
300 suberoylanilide hydroxamic acid increased tubulin acetylation and consequently improved
301 autophagic function in human fibroblasts, in the context of Cockayne syndrome (Majora et al.
302 2018).

303 Results obtained in this study indicate that HDAC6 inhibition, or knockdown, reduced
304 levels of active NF- κ B as well as the expression of inflammatory markers (ICAM-1, VCAM-1
305 and MCP-1) in endothelial cells exposed to low SS. These findings are in accordance with
306 previous work which demonstrated an anti-inflammatory effect of Tubastatin-A in epithelial
307 cells, *via* the regulation of the NF- κ B pathway (Wang et al. 2018). Other studies have shown that
308 HDAC6 inhibition downregulates the production of inflammatory cytokines, such as IL-6, IL-1 β ,
309 and TNF- α in murine models of arthritis and synovial inflammation, and Freund's complete
310 adjuvant-induced mouse model of inflammation (Ran and Zhou 2019). HDAC6 inhibition has
311 also been reported to reduce TNF- α -induced endothelial dysfunction and prolong survival in
312 murine models of systemic inflammation and injury (Yu et al. 2016). Though the underlying
313 mechanisms seem to be multiple and complex, we found that the autophagic machinery played a
314 central role in endothelial cells. Indeed, reducing levels of the essential autophagy protein ATG5,
315 significantly reduced LC3-lipidation and suppressed the anti-inflammatory effects of HDAC6-
316 inhibition by approximately 70%. This indicates that a functional autophagic process is key to
317 relaying these beneficial effects and is in line with our previous data showing that autophagy is
318 required for atheroprotection under physiological blood flow (Vion et al. 2017). Efficient
319 autophagy may favor an anti-inflammatory endothelial phenotype by limiting the accumulation
320 of damaged organelles, protein aggregates or intracellular pathogens (Mai et al. 2012; Cadwell
321 2016) and by limiting NF- κ B signaling (Peng et al. 2019).

322

323 To further assess the role of HDAC6 in atherosclerotic plaque formation, we used a double
324 knockout murine model, *HDAC6*^{-/-}/*ApoE*^{-/-}. As previously described *HDAC6*^{-/-} animals were
325 viable and showed no signs of major defects (Zhang et al. 2008). These mice, and their control
326 littermates, underwent bone marrow transplantation, which allowed us to focus on the role
327 played by resident cells in the vasculature in the development of atherosclerotic plaques. We
328 found that knocking out *HDAC6* reduced atherosclerotic plaque development in the low SS areas
329 of hypercholesterolemic mice. These effects were not caused by other systemic metabolic
330 parameters influencing cardiovascular risk, as plasma cholesterol levels, body weight and blood
331 cell count were not affected by *HDAC6* knockout. In addition to clearing damaged intracellular
332 material, restoring autophagic flux in endothelial cells exposed to low shear stress, may also aid
333 in their ability to limit lipid accumulation and the subsequent inflammatory response (Torisu et
334 al. 2016; Kim et al. 2020). Alternatively, data by Manea et al indicated that administering
335 suberoylanilide hydroxamic acid to hypercholesterolemic mice reduced the progression of
336 atherosclerotic lesions through the reduction of oxidative stress in the aorta (Manea et al. 2020).
337 Furthermore, Chen et al. (2019) found showed that another HDAC6 inhibitor (Tubacin)
338 mitigates endothelial dysfunction by regulating expression of endothelial nitric oxide synthetase
339 (J. Chen et al. 2019). Whether or not these alternate pathways are linked to the autophagic
340 machinery requires further investigation. While our focus in this study has been on endothelial
341 cells, we cannot exclude that autophagy stimulation may also occur in smooth muscle cells via
342 *HDAC6*-knockout. This very well might contribute to the anti-atherogenic effects we observed in
343 our *in vivo* experimental model, since defective autophagy in vascular smooth muscle cells has
344 been linked to accelerated atherogenesis (Grootaert et al. 2015).

345 Collectively, the main findings of this study indicate that targeting HDAC6 stimulates
346 autophagic flux, decreases markers of inflammation in endothelial cells, and the formation of
347 atherosclerotic lesions in mice. These results bolster the idea that autophagy-stimulating
348 strategies might be beneficial in treating atherosclerosis, and present HDAC6-oriented
349 interventions as an interesting route.

350

351 **Acknowledgement:** The authors acknowledge Cecile Devue for her helpful contributions, Flow
352 Cytometry Facility manager, Dr Camille Knosp, as well as members of the INSERM U970
353 Histology, Microscopy and ERI facilities.

354

355 **Funding:** This work has been supported by INSERM and a grant from the French National
356 Agency for Research ANR-16-CE14-0015-01 and from the Fondation pour la Recherche
357 Médicale (FRM EQU202003010767). S.C. was supported by the USPC Inspire Program

358 European Union's Horizon 2020 research and innovation program under the Marie Skłodowska-
359 Curie grant agreement No 665850. T.A.M. received funding from National Institute of Health by
360 grants HL116848, HL147558, DK119594, HL127240, HL150225, and a grant from the
361 American Heart Association (16SFRN31400013). T.A.M. is on the scientific advisory board of
362 Artemes Bio, Inc., received funding from Italfarmaco for an unrelated project, and has a
363 subcontract from Eikonizo Therapeutics related to an SBIR grant from the National Institutes of
364 Health (HL154959).

365
366 **Conflict of interest:** All authors declare nothing to disclose

367

368 **MATERIAL AND METHODS**

369 **Human Umbilical Vein Endothelial cells (HUVECs)**

370 HUVECs were obtained from 20 different donors (11 males, 9 females) (PromoCell; Heidelberg,
371 Germany). Cells were plated at a density of 10,000 cells/cm² and cultured in Endothelial Cell
372 Basal Medium (ECBM, PromoCell; Heidelberg, Germany), supplemented with 2% Fetal Calf
373 Serum (PromoCell; Heidelberg, Germany), growth factors (0.4% ECGS, 0.1 ng/mL EGF, 1
374 ng/mL β -FGF), 90 μ g/mL heparin, 1 μ g/mL hydrocortisone, 10 μ g/L Amphotericin B (Gibco™ -
375 15290026), 100 IU/mL Streptomycin (Gibco™-15140148) and 100 IU/mL Penicillin (Gibco™-
376 15140148). Confluent cells were detached with 0.025% Trypsin-EDTA (Gibco™ - 25300-054)
377 in PBS (Gibco™ - 10010023) for 5min at 37°C, followed by washing with complete medium
378 and centrifuging at 600g for 10min.

379

380 **Lentiviral transduction**

381 Lentiviruses expressing inducible shRNA (Sigma-Aldrich, MISSION™ shRNA inducible
382 vectors) were used to silence HDAC and ATG5. Cells were infected with lentivirus carrying
383 shHDAC6/shATG5 or shControl at MOI 5 for 24 hours in the presence of Hexamethidine
384 Bromide (8 μ g/mL; Sigma-Aldrich - H9268). Transduced cells were selected using puromycin
385 (Sigma Aldrich #P9620) at 1 μ g/mL. HUVECs were treated for about 10 days with Isopropyl β -
386 D-1-thiogalactopyranoside (IPTG; Sigma-Aldrich - I6758) at 1mmol/mL.

387

388 ***In Vitro* shear stress system**

389 Confluent HUVECs from passage 2-4 were cultured on glass slides coated with 0.2% gelatin,
390 and placed in a parallel plate chamber perfused with circulating medium for 24 hours, under
391 laminar flow as described earlier (Vion et al. 2017). When specifically stated, cells were treated
392 with Tubastatin-A (3 μ M, Sigma-Aldrich), Rapamycin (1 μ M; Sigma-Aldrich) or Chloroquine
393 (Sigma-Aldrich C6628) and exposed for 24 hours under shear stress conditions. For control

394 conditions, HUVECs were exposed to vehicle (Dimethyl Sulphoxide; 0.1 μ L/mL, Sigma-
395 Aldrich). For inflammation studies, the cells were treated with TNF- α (1 ng/mL, Peprotech) for
396 the last 12 hours of the experiment.

397

398 **Western blot analysis**

399 HUVECs were immediately washed twice with PBS and lysed in Radioimmunoprecipitation
400 assay (RIPA) buffer consisting of 150 mmol/L NaCl, 50 mmol/L Tris HCl (pH=7.4), 2 mmol/L
401 EDTA, 2 mmol/L activated orthovanadate, 0.5% deoxycholate, 0.2% Sodium Dodecyl Sulphate
402 and supplemented with CompleteTM Mini protease and phosphatase inhibitors cocktails (Roche,
403 France). Then, the lysates were centrifuged for 15 minutes at 12500g, 4°C to remove cell debris.
404 The supernatant was collected and stored at -80°C until further analysis. Protein concentration
405 was estimated by Lowry's protein assay method (DCTM Protein Assay, BioRad).

406 Protein samples were denatured using buffer containing Tris-carboxyethyl phosphine
407 hydrochloride (20x XT-Reducing Agent, BioRad-1610792) and separated based on molecular
408 weight by electrophoresis in 4-12% gradient gels (CriterionTM, BioRad-3450123). Proteins were
409 then transferred on either 0.45 μ m nitrocellulose (BioRad) or Polyvinylidene Fluoride (PVDF)
410 membranes; following which the membranes were incubated with Ponceau Red to verify the
411 efficiency of the transfer process. Membranes were blocked with 5% (w/v) milk or Bovine
412 Serum Albumin (BSA) in TBS supplemented with 0.1% Tween-20. To detect the protein of
413 interest, membranes were then incubated with primary antibodies overnight at 4°C, with constant
414 agitation (*Supplementary Table 1*). After three 10-minute washes, the membranes were incubated
415 with secondary antibody coupled with Horseradish Peroxidase (anti-rabbit, anti-rat or anti-
416 mouse, Amersham, GE Healthcare, 1/3000) for 1 hour at room temperature. Immunodetection
417 was performed using ClarityTM Western ECL Substrate, and the chemiluminescent signal was
418 revealed using the Las-4000 imaging system and quantified with MultiGauge software (Fujifilm,
419 Japan)

420

421

422

423 **Immunofluorescence**

424 Cells were fixed with either 100% ice-cold methanol for 20 minutes at -20°C or 4% (v/v)
425 paraformaldehyde (PFA) in PBS, for 5 minutes at room temperature. Cells fixed with PFA were
426 permeabilized with 0.1% Triton X-100 for 10 minutes at room temperature. Permeabilized cells
427 were blocked with 5% (w/v) BSA in PBS for 30 minutes and then incubated with primary

428 antibody overnight at 4°C (*Supplementary Table 2*). The cells were washed with PBS and
429 incubated with secondary antibody conjugated with fluorescent dye, Alexa Fluor[®]. Lastly, the
430 nuclei were labeled with DAPI. The labeled cells were mounted on coverslips using
431 Fluoromount-G[®].

432 To perform *en face* immunostaining, aortas were harvested from mice and fixed with ice-cold
433 4% (v/v) PFA for 20 minutes. Residual fat attached to the aorta was removed and dissected along
434 the entire inner side and outer curvature of the arch. Aortas were then blocked with 5% (w/v)
435 BSA in PBS, for 60 minutes at room temperature, and incubated with primary antibody for
436 overnight, 4°C. Following incubation with primary antibody, the aortas were washed multiple
437 times and incubated with secondary antibody conjugated with Alexa Fluor[®] for 2 hours at room
438 temperature. Subsequently, the aortas were washed with PBS and the nuclei were labeled with
439 DAPI. Labeled aortas were transferred onto glass slides and mounted “*en face*”. The slides
440 prepared were examined using Leica SP8 confocal microscope and analyzed with software
441 ImageJ. For colocalization analysis, ImageJ PlugIn ‘*Colocalization Finder*’ was used and
442 Manders’ coefficients were calculated.

443

444 **Deacetylase activity assay**

445 To determine the deacetylase enzymatic activity of HDAC6, a fluorescence-based assay was
446 performed (Lemon et al. 2011). Deacetylation of substrate by HDAC6 sensitizes the substrate to
447 the developer solution, which generates a fluorophore. The fluorescence signal is then detected
448 by a fluorimetric plate reader at 460 nm. HUVECs were lysed in PBS buffer supplemented with
449 - 0.5% Triton X-100, 300 mM NaCl and protease/phosphatase inhibitor cocktail (Thermo
450 Fisher). Lysed cells were sonicated and centrifuged at 12500g for 15 minutes, 4°C. The pellet
451 was discarded, and the supernatant was transferred to fresh tubes. Protein concentration was
452 estimated by Micro BCA assay (Thermo Scientific[™] - 23235). For the assay, 15 µg of lysates
453 were diluted in 100 µL of PBS and added to a 96-well plate. Where required, 1 µL of the 100x
454 HDAC6 inhibitor of the stock solution were added. Vehicle (DMSO) was added to the controls
455 at the same concentration. The plates were incubated at 37°C for 60 minutes. 5 µL of substrate,
456 specific to HDAC Class II, were added to the wells at a concentration of 1mM and incubated for
457 2 hours at 37°C. Substrate was bought from Bachem (I-1875; Boc-Lys (Ac)-AMC). 50 µL per
458 well, developer solution was added and incubated at 37°C for 20 minutes. The developer
459 solution consisted of 1.5% Triton X-100, 3 µM TSA (Sigma-Aldrich, T8552), and 0.75 mg/mL
460 trypsin (Gibco[™] 15400054), diluted in 1x PBS. AMC fluorescence was measured using a plate

461 reader, with excitation and emission filters of 360 nm and 460 nm, respectively. Background
462 signals corresponding to the blank solutions was subtracted.

463

464

465 **Monitoring autophagic flux using mRFP-GFP-LC3**

466 In order to observe the effect of shear stress on endothelial autophagic flux, we used a LC3
467 protein, fluorescently tagged with a RFP- GFP tandem, (generous gift from Dr F. Oury, Inserm
468 Paris), according to Vion Kheloufi et al, PNAS 2017 (Vion et al. 2017). The tandem allows us to
469 observe different stages autophagy. At the autophagosomes stage, the LC3 protein is visualized
470 as yellow signal, due to the overlapping of green and red fluorescence signal from GFP and RFP.
471 However, when autolysosomes are formed, the acidic pH from lysosomes causes quenching of
472 GFP. Therefore, the red fluorescent signal corresponds to LC3 present only in the autolysosomes
473 stage. The cells were infected with lentiviruses carrying the plasmid (MOI = 6) in the presence of
474 Hexamethidine Bromide (8 µg/mL; Sigma-H9268) for 24 hours. HUVECs were then exposed to
475 shear stress for 24 hours with or without Tubastatin-A (3 µM; Sigma-SML0044). For
476 experiments where autophagic flux was blocked, HUVECs were treated with Chloroquine
477 (300µM) for the last 6 hours of the shear stress. After exposure to shear stress, the cells were
478 washed with PBS and fixed with 4% PFA for 5 minutes at room temperature, followed by
479 labeling the nuclei with DAPI. The slides were mounted using Fluoromount-G[®]
480 (SouthernBiotech). Images of the prepared slides were taken with the Leica SP8 confocal
481 microscope and analyzed for LC3 positive signal using ImageJ software.

482

483 **ELISA**

484 Levels of Monocyte Chemoattractant Protein-1 (MCP-1), released by HUVECs, in the media,
485 were assessed by ELISA (R&D, Human MCP-1 Duo-Set DY279). The assay was performed
486 according to manufacturer's protocol.

487

488 **Animal model**

489 All the mice used in the study were of C57BL/6 genetic background. The double knockout
490 model was generated by crossing *HDAC6*^{-/-} mice, provided by T. McKinsey, University
491 Colorado Denver, USA, and *ApoE*^{-/-} (Charles River Laboratories). All experiments were
492 performed in accordance with the European Community guidelines for the care and use of
493 laboratory animals (no. 07430) and were approved by the institutional ethical committee (no.
494 02526.02). All experiments were performed on male mice. Since the *HDAC6* gene is found on

495 the X-chromosome, it was possible to obtain only male littermate control mice to be used for the
496 experiments.

497

498 **Bone Marrow Transplant**

499 8 weeks old *HDAC6^{-/-}/ApoE^{-/-}* and *HDAC6^{+/+}/ApoE^{-/-}* male mice underwent Bone Marrow
500 Transplant (BMT) procedure, in order to replenish the bone marrow in the mutated models with
501 *HDAC6^{+/+}/ApoE^{-/-}* donor bone marrow. This allowed us to focus on the role of endothelial cells
502 and rule out the potential function of hematopoietic cells in progression of atherosclerosis. 4-6
503 weeks old *HDAC6^{+/+}/ApoE^{-/-}* donor mice were euthanized by cervical dislocation and the bone
504 marrow was extracted from tibia and femur. The bone marrow was flushed and filtered. The
505 recipient mice received radiation, 9.5 Gray, and were transplanted with donor bone marrow by
506 retro-orbital injections the day after. The mice were allowed to recover for 4 weeks, following
507 which they were put on high fat diet (D12079B, Research Diets; 20% proteins, 50% glucose,
508 21% lipids). After 10 weeks of high fat diet, the mice were euthanized.

509

510

511 **Evaluation of Blood Cholesterol Levels**

512 Mice were anesthetized with 2% isoflurane and blood (75 μ L) was collected by making a sub-
513 mandibular puncture. To prepare platelet-free plasma, the blood collected was centrifuged twice
514 at 2500g for 15 minutes at room temperature. The cholesterol content was determined using
515 Cholesterol FS 10' kit (Diasys).

516

517 **Isolation of Aortas**

518 Mice were anesthetized using isoflurane (flow was set at 2.5% for induction and 2% for
519 maintenance) and 2L/min of O₂. The abdominal organs were moved aside to expose the inferior
520 *vena cava*. 500- μ L blood was drawn from the inferior *vena cava* using a 1 mL syringe and 26G
521 needle primed with sodium citrate. Following blood collection, the diaphragm was cut, and the
522 thoracic cavity exposed. The right atrium was nicked to release the blood. The heart was flushed
523 with PBS via the left ventricle, using a 10 mL syringe and 25G needle. Followed by PBS, the
524 heart was flushed with 1-2 mL ice-cold 4% PFA and PBS to wash out the excess PFA. To allow
525 for better access to the aorta, the liver, lungs, trachea, oesophagus, thymus gland and pulmonary
526 artery, were removed. Using micro-dissection scissors and forceps the excess adipose tissue and
527 adventitia, surrounding the thoracic aorta and the carotids, were removed. The clean aorta was

528 excised from the heart and placed in 4% PFA for 20 minutes on ice, followed by storage in ice-
529 cold PBS.

530

531 **Determination of Atherosclerotic Plaque Size On *En Face* Aortas**

532 The aortas were then stained with freshly prepared Oil Red O dye (40% distilled water, 60% Oil
533 Red O solution) for 20 minutes with constant agitation. The solution was prepared by dissolving
534 the dye in isopropanol at a concentration of 5g/L. The aortas were washed with 75% ethanol for
535 5 minutes to remove the excess stain and mounted “*en face*” on glass slides and observed under
536 microscope. Surface area occupied by the plaque was assessed using software, ImageJ.

537

538 **Preparation of Spleen**

539 Spleens were then weighed and rinsed twice with ice-cold 0.1 μm filtered PBS containing 3%
540 FBS. Placing them on 3% PBS-FBS pre-wetted 40 μm nylon cell strainers (Cat#352340, Thermo
541 Fisher Scientific, USA) suspended over a 50 mL polypropylene tube, the spleens were then
542 mashed using the plunger end of a 1 mL syringe. The cell strainers were then rinsed four times
543 with 1 mL of 3% PBS-FBS. Cell suspension was then centrifuged at 500xg for 10 minutes at
544 4°C. The supernatant was then carefully aspirated and discarded, and the pellet was then
545 resuspended in 1 mL of 0.1 μm filtered PBS. 1 mL of red blood cell lysis buffer (Cat# R7757,
546 Merck, USA) was added to the resuspension and incubated at 5 minutes at room temperature.
547 After the incubation, 18 mL of 3% PBS-FBS was added and suspension was centrifuged at 500g
548 for 10 minutes at 4°C. Supernatant was then removed carefully, and pellet was resuspended in 3
549 mL of complete RPMI media that consisted of RPMI 1640 Medium with GlutaMAX and
550 HEPES (Cat# 72400021, Thermo Fisher Scientific, USA) supplemented with 10% FBS, 1% P/S
551 and 0.1% β -mercaptoethanol (Cat# 1610710, Bio-Rad, USA). Cells were then counted, and a
552 final concentration of 10×10^6 cells/mL was obtained.

553

554 **Preparation of Bone Marrow**

555 The femur and tibia were isolated from the hind legs of the mouse. Sterilized micronic tubes,
556 with a pore at the bottom, were placed in 1.5 mL Eppendorf tubes. One bone was placed per tube
557 and centrifuged at 10000g for 15 seconds at room temperature. Collected cells were resuspended
558 in 800 μL PBS, passed through 40micron syringe filter. The samples were then centrifuged at
559 400g for 10 minutes at 4°C. The pellet was resuspended in PBS to have a concentration of
560 10×10^6 cells/mL. Bone marrow cells were incubated with the antibody mix for 30 minutes at

561 4°C. The plate was centrifuged at 500g for 5 minutes at 4°C. The pellet was resuspended in 100
562 µL of 1% PBS-FBS.

563

564 **Flow Cytometry**

565 Circulating and splenic immune cell populations were defined as follows: NK cells as NK1.1⁺,
566 neutrophils as CD11b⁺/Ly6C⁺/Ly6G⁺, monocytes as CD11b⁺/Ly6C⁺/Ly6G⁻, dendritic cells as
567 CD11b⁺/Ly6C⁺/Ly6G⁻/CD11c⁺, macrophages as CD11b^{lo/-}/Ly6c⁺/Ly6g⁻/F480^{hi}, activated mature
568 B lymphocytes as CD19⁺/IgM⁺/B220⁺, cytotoxic T lymphocytes as CD3⁺/CD8⁺ and helper T
569 lymphocytes as CD3⁺/CD4⁺. Antibody incubation was performed on ice for 30 minutes
570 (supplemental Table 3) in 96-well plate and 100 µl of PBS-FBS 1% was added post-incubation.
571 The plate was then centrifuged at 500g for 5 minutes at 4°C and supernatant was removed by
572 inverting the plate. A final resuspension of splenocyte pellet with 100 µl of PBS-FBS 1% was
573 performed before transfer to Micronic tubes (Cat# 2517810, Dutscher, France) for flow
574 cytometry analysis (LSRFortessa™, BD Biosciences, USA). Data was analyzed using FlowJo
575 software (BD Biosciences, USA).

576

577 **Statistical Analysis**

578 Data are expressed as mean ± SEM for all experiments. Comparisons between different SS
579 conditions or between control and treatment conditions were performed by using a Wilcoxon test
580 for *in vitro experiments*. Comparisons between groups of mice were performed by using the
581 Mann–Whitney *U* test or 2-way Anova (with Sidak post-hoc test). Statistical analyses were
582 performed using the GraphPad Prism 7 statistical package. All tests were two-sided and used a
583 significance level of 0.05.

584

585 **REFERENCES**

- 586 1. Baeyens, Nicolas, Chiroree Bandyopadhyay, Brian G. Coon, Sanguk Yun, and Martin A.
587 Schwartz. 2016. “Endothelial Fluid Shear Stress Sensing in Vascular Health and Disease.”
588 *Journal of Clinical Investigation* 126 (3): 821–28. <https://doi.org/10.1172/JCI83083>.
- 589 2. Bailey, Keith A., Fawaz G. Haj, Scott I. Simon, and Anthony G. Passerini. 2017.
590 “Atherosusceptible Shear Stress Activates Endoplasmic Reticulum Stress to Promote
591 Endothelial Inflammation.” *Scientific Reports* 7 (1): 8196. <https://doi.org/10.1038/s41598-017-08417-9>.
- 593 3. Bánrési, Ágnes, Miklós Sass, and Yacine Graba. 2013. “The Emerging Role of Acetylation in
594 the Regulation of Autophagy.” *Autophagy* 9 (6): 819–29. <https://doi.org/10.4161/auto.23908>.
- 595 4. Birdsey, Graeme M., Nicola H. Dryden, Aarti V. Shah, Rebecca Hannah, Matthew D. Hall,
596 Dorian O. Haskard, Maddy Parsons, et al. 2012. “The Transcription Factor Erg Regulates
597 Expression of Histone Deacetylase 6 and Multiple Pathways Involved in Endothelial Cell
598 Migration and Angiogenesis.” *Blood* 119 (3): 894–903. [19](https://doi.org/10.1182/blood-2011-</p></div><div data-bbox=)

- 599 04-350025.
- 600 5. Borgas, Diana, Eboni Chambers, Julie Newton, Junsuk Ko, Stephanie Rivera, Sharon
601 Rounds, and Qing Lu. 2016. "Cigarette Smoke Disrupted Lung Endothelial Barrier Integrity
602 and Increased Susceptibility to Acute Lung Injury via Histone Deacetylase 6." *American
603 Journal of Respiratory Cell and Molecular Biology* 54 (5): 683–96.
604 <https://doi.org/10.1165/rcmb.2015-0149OC>.
- 605 6. Butler, Kyle V., Jay Kalin, Camille Brochier, Giulio Vistoli, Brett Langley, and Alan P.
606 Kozikowski. 2010. "Rational Design and Simple Chemistry Yield a Superior,
607 Neuroprotective HDAC6 Inhibitor, Tubastatin A." *Journal of the American Chemical Society*
608 132 (31): 10842–46. <https://doi.org/10.1021/ja102758v>.
- 609 7. Cadwell, Ken. 2016. "Crosstalk between Autophagy and Inflammatory Signalling Pathways:
610 Balancing Defence and Homeostasis." *Nature Reviews. Immunology* 16 (11): 661–75.
611 <https://doi.org/10.1038/nri.2016.100>.
- 612 8. Chen, Jihui, Jian Zhang, Noor F. Shaik, Bing Yi, Xin Wei, Xiao-Feng Yang, Ulhas P. Naik,
613 et al. 2019. "The Histone Deacetylase Inhibitor Tubacin Mitigates Endothelial Dysfunction
614 by Up-Regulating the Expression of Endothelial Nitric Oxide Synthase." *Journal of
615 Biological Chemistry* 294 (51): 19565–76. <https://doi.org/10.1074/jbc.RA119.011317>.
- 616 9. Chen, Sigeng, Geoffrey C. Owens, Helen Makarenkova, and David B. Edelman. 2010.
617 "HDAC6 Regulates Mitochondrial Transport in Hippocampal Neurons." Edited by Colin
618 Combs. *PLoS ONE* 5 (5): e10848. <https://doi.org/10.1371/journal.pone.0010848>.
- 619 10. Chiu, Jeng-Jiann, and Shu Chien. 2011. "Effects of Disturbed Flow on Vascular
620 Endothelium: Pathophysiological Basis and Clinical Perspectives." *Physiological Reviews* 91
621 (1): 327–87. <https://doi.org/10.1152/physrev.00047.2009>.
- 622 11. Chiu, Jeng-Jiann, Pei-Ling Lee, Cheng-Nan Chen, Chih-I Lee, Shun-Fu Chang, Li-Jing
623 Chen, Sheng-Chieh Lien, Ya-Chen Ko, Shunichi Usami, and Shu Chien. 2004. "Shear Stress
624 Increases ICAM-1 and Decreases VCAM-1 and E-Selectin Expressions Induced by Tumor
625 Necrosis Factor- α in Endothelial Cells." *Arteriosclerosis, Thrombosis, and Vascular Biology*
626 24 (1): 73–79. <https://doi.org/10.1161/01.ATV.0000106321.63667.24>.
- 627 12. Du, Yifeng, Michael L. Seibenhener, Jin Yan, Jianxiong Jiang, and Michael C. Wooten.
628 2015. "APKC Phosphorylation of HDAC6 Results in Increased Deacetylation Activity."
629 *PLoS ONE* 10 (4). <https://doi.org/10.1371/journal.pone.0123191>.
- 630 13. Eshun-Wilson, Lisa, Rui Zhang, Didier Portran, Maxence V. Nachury, Daniel B. Toso,
631 Thomas Löhr, Michele Vendruscolo, Massimiliano Bonomi, James S. Fraser, and Eva
632 Nogales. 2019. "Effects of α -Tubulin Acetylation on Microtubule Structure and Stability."
633 *Proceedings of the National Academy of Sciences* 116 (21): 10366–71.
634 <https://doi.org/10.1073/pnas.1900441116>.
- 635 14. Feng, Yuchen, Ding He, Zhiyuan Yao, and Daniel J Klionsky. 2014. "The Machinery of
636 Macroautophagy." *Cell Research* 24 (1): 24–41. <https://doi.org/10.1038/cr.2013.168>.
- 637 15. Geeraert, Camille, Ameetha Ratier, Simon G. Pfisterer, Daniel Perdiz, Isabelle Cantaloube,
638 Audrey Rouault, Sophie Patingre, Tassula Proikas-Cezanne, Patrice Codogno, and Christian
639 Poüs. 2010. "Starvation-Induced Hyperacetylation of Tubulin Is Required for the Stimulation
640 of Autophagy by Nutrient Deprivation." *Journal of Biological Chemistry* 285 (31): 24184–
641 94. <https://doi.org/10.1074/jbc.M109.091553>.
- 642 16. Grootaert, Mandy Oj, Paula A. da Costa Martins, Nicole Bitsch, Isabel Pintelon, Guido Ry
643 De Meyer, Wim Martinet, and Dorien M. Schrijvers. 2015. "Defective Autophagy in
644 Vascular Smooth Muscle Cells Accelerates Senescence and Promotes Neointima Formation
645 and Atherogenesis." *Autophagy* 11 (11): 2014–32.
646 <https://doi.org/10.1080/15548627.2015.1096485>.
- 647 17. Guo, Feng-Xia, Yan-Wei Hu, Lei Zheng, and Qian Wang. 2017. "Shear Stress in Autophagy
648 and Its Possible Mechanisms in the Process of Atherosclerosis." *DNA and Cell Biology* 36
649 (5): 335–46. <https://doi.org/10.1089/dna.2017.3649>.

- 650 18. Kim, Hae-Suk, Guang Ren, Teayoun Kim, Sushant Bhatnagar, Qinglin Yang, Young Yil
651 Bahk, and Jeong-a Kim. 2020. "Metformin Reduces Saturated Fatty Acid-Induced Lipid
652 Accumulation and Inflammatory Response by Restoration of Autophagic Flux in Endothelial
653 Cells." *Scientific Reports* 10 (1): 13523. <https://doi.org/10.1038/s41598-020-70347-w>.
- 654 19. Köchl, Robert, Xiao Wen Hu, Edmond Y. W. Chan, and Sharon A. Tooze. 2006.
655 "Microtubules Facilitate Autophagosome Formation and Fusion of Autophagosomes with
656 Endosomes: Role of Microtubules in AV Formation." *Traffic* 7 (2): 129–45.
657 <https://doi.org/10.1111/j.1600-0854.2005.00368.x>.
- 658 20. Lee, Ding-Yu, and Jeng-Jiann Chiu. 2019. "Atherosclerosis and Flow: Roles of Epigenetic
659 Modulation in Vascular Endothelium." *Journal of Biomedical Science* 26 (1): 56.
660 <https://doi.org/10.1186/s12929-019-0551-8>.
- 661 21. Lemon, Douglas D., Todd R. Horn, Maria A. Cavasin, Mark Y. Jeong, Kurt W. Haubold,
662 Carlin S. Long, David C. Irwin, et al. 2011. "Cardiac HDAC6 Catalytic Activity Is Induced
663 in Response to Chronic Hypertension." *Journal of Molecular and Cellular Cardiology* 51
664 (1): 41–50. <https://doi.org/10.1016/j.yjmcc.2011.04.005>.
- 665 22. Levy, Jean M. Mulcahy, Christina G. Towers, and Andrew Thorburn. 2017. "Targeting
666 Autophagy in Cancer." *Nature Reviews Cancer* 17 (9): 528–42.
667 <https://doi.org/10.1038/nrc.2017.53>.
- 668 23. Mackeh, R., D. Perdiz, S. Lorin, P. Codogno, and C. Pous. 2013. "Autophagy and
669 Microtubules - New Story, Old Players." *Journal of Cell Science* 126 (5): 1071–80.
670 <https://doi.org/10.1242/jcs.115626>.
- 671 24. Mai, Sören, Britta Muster, Jürgen Bereiter-Hahn, and Marina Jendrach. 2012. "Autophagy
672 Proteins LC3B, ATG5 and ATG12 Participate in Quality Control after Mitochondrial
673 Damage and Influence Lifespan." *Autophagy* 8 (1): 47–62.
674 <https://doi.org/10.4161/auto.8.1.18174>.
- 675 25. Majora, Marc, Kevin Sondenheimer, Maren Knechten, Ingo Uthe, Charlotte Esser, Alfonso
676 Schiavi, Natascia Ventura, and Jean Krutmann. 2018. "HDAC Inhibition Improves
677 Autophagic and Lysosomal Function to Prevent Loss of Subcutaneous Fat in a Mouse Model
678 of Cockayne Syndrome." *Science Translational Medicine* 10 (456): eaam7510.
679 <https://doi.org/10.1126/scitranslmed.aam7510>.
- 680 26. Manea, Simona-Adriana, Mihaela-Loredana Vlad, Ioana Madalina Fenyo, Alexandra-Gela
681 Lazar, Monica Raicu, Horia Muresian, Maya Simionescu, and Adrian Manea. 2020.
682 "Pharmacological Inhibition of Histone Deacetylase Reduces NADPH Oxidase Expression,
683 Oxidative Stress and the Progression of Atherosclerotic Lesions in Hypercholesterolemic
684 Apolipoprotein E-Deficient Mice; Potential Implications for Human Atherosclerosis." *Redox*
685 *Biology* 28 (January): 101338. <https://doi.org/10.1016/j.redox.2019.101338>.
- 686 27. Mauthe, Mario, Idil Orhon, Cecilia Rocchi, Xingdong Zhou, Morten Luhr, Kerst-Jan
687 Hijlkema, Robert P. Coppes, Nikolai Engedal, Muriel Mari, and Fulvio Reggiori. 2018.
688 "Chloroquine Inhibits Autophagic Flux by Decreasing Autophagosome-Lysosome Fusion."
689 *Autophagy* 14 (8): 1435–55. <https://doi.org/10.1080/15548627.2018.1474314>.
- 690 28. McCue, Shannon, Dorota Dajnowiec, Feng Xu, Ming Zhang, Moira R. Jackson, and B.
691 Lowell Langille. 2006. "Shear Stress Regulates Forward and Reverse Planar Cell Polarity of
692 Vascular Endothelium In Vivo and In Vitro." *Circulation Research* 98 (7): 939–46.
693 <https://doi.org/10.1161/01.RES.0000216595.15868.55>.
- 694 29. Mialet-Perez, Jeanne, and Cécile Vindis. 2017. "Autophagy in Health and Disease: Focus on
695 the Cardiovascular System." Edited by Jon D. Lane, Viktor I. Korolchuk, and James T.
696 Murray. *Essays in Biochemistry* 61 (6): 721–32. <https://doi.org/10.1042/EBC20170022>.
- 697 30. Mizushima, Noboru. 2018. "A Brief History of Autophagy from Cell Biology to Physiology
698 and Disease." *Nature Cell Biology* 20 (5): 521–27. [https://doi.org/10.1038/s41556-018-0092-](https://doi.org/10.1038/s41556-018-0092-5)
699 5.
- 700 31. Mizushima, Noboru, Beth Levine, Ana Maria Cuervo, and Daniel J. Klionsky. 2008.

- 701 “Autophagy Fights Disease through Cellular Self-Digestion.” *Nature* 451 (7182): 1069–75.
702 <https://doi.org/10.1038/nature06639>.
- 703 32. Peng, Xuan, Yating Wang, Huiyan Li, Jinjin Fan, Jiani Shen, Xueqing Yu, Yi Zhou, and
704 Haiping Mao. 2019. “ATG5-Mediated Autophagy Suppresses NF-KB Signaling to Limit
705 Epithelial Inflammatory Response to Kidney Injury.” *Cell Death & Disease* 10 (4): 253.
706 <https://doi.org/10.1038/s41419-019-1483-7>.
- 707 33. Ran, Jie, and Jun Zhou. 2019. “Targeted Inhibition of Histone Deacetylase 6 in Inflammatory
708 Diseases.” *Thoracic Cancer* 10 (3): 405–12. <https://doi.org/10.1111/1759-7714.12974>.
- 709 34. Ravikumar, Brinda, Abraham Acevedo-Arozena, Sara Imarisio, Zdenek Berger, Coralie
710 Vacher, Cahir J O’Kane, Steve D M Brown, and David C Rubinsztein. 2005. “Dynein
711 Mutations Impair Autophagic Clearance of Aggregate-Prone Proteins.” *Nature Genetics* 37
712 (7): 771–76. <https://doi.org/10.1038/ng1591>.
- 713 35. Souilhol, Celine, Jovana Serbanovic-Canic, Maria Fragiadaki, Timothy J. Chico, Victoria
714 Ridger, Hannah Roddie, and Paul C. Evans. 2020. “Endothelial Responses to Shear Stress in
715 Atherosclerosis: A Novel Role for Developmental Genes.” *Nature Reviews Cardiology* 17
716 (1): 52–63. <https://doi.org/10.1038/s41569-019-0239-5>.
- 717 36. Torisu, Kumiko, Krishna K. Singh, Takehiro Torisu, Fina Lovren, Jie Liu, Yi Pan, Adrian
718 Quan, et al. 2016. “Intact Endothelial Autophagy Is Required to Maintain Vascular Lipid
719 Homeostasis.” *Aging Cell* 15 (1): 187–91. <https://doi.org/10.1111/acer.12423>.
- 720 37. Ustinova, Kseniya, Zora Novakova, Makoto Saito, Marat Meleshin, Jana Mikesova, Zsofia
721 Kutil, Petra Baranova, et al. 2020. “The Disordered N-Terminus of HDAC6 Is a
722 Microtubule-Binding Domain Critical for Efficient Tubulin Deacetylation.” *Journal of*
723 *Biological Chemistry* 295 (9): 2614–28. <https://doi.org/10.1074/jbc.RA119.011243>.
- 724 38. Vion, Anne-Clemence, Marouane Kheloufi, Adel Hammoutene, Johanne Poisson, Juliette
725 Lasselin, Cecile Devue, Isabelle Pic, et al. 2017. “Autophagy Is Required for Endothelial
726 Cell Alignment and Atheroprotection under Physiological Blood Flow.” *Proceedings of the*
727 *National Academy of Sciences* 114 (41): E8675–84.
728 <https://doi.org/10.1073/pnas.1702223114>.
- 729 39. Wang, Jingjing, Lilei Zhao, Zhengkai Wei, Xu Zhang, Yanan Wang, Fan Li, Yunhe Fu, and
730 Bin Liu. 2018. “Inhibition of Histone Deacetylase Reduces Lipopolysaccharide-Induced-
731 Inflammation in Primary Mammary Epithelial Cells by Regulating ROS-NF-KB Signaling
732 Pathways.” *International Immunopharmacology* 56 (March): 230–34.
733 <https://doi.org/10.1016/j.intimp.2018.01.039>.
- 734 40. Wen, Xin, and Daniel J. Klionsky. 2016. “An Overview of Macroautophagy in Yeast.”
735 *Journal of Molecular Biology* 428 (9): 1681–99. <https://doi.org/10.1016/j.jmb.2016.02.021>.
- 736 41. Wong, Alan S.L., Zelda H. Cheung, and Nancy Y. Ip. 2011. “Molecular Machinery of
737 Macroautophagy and Its Deregulation in Diseases.” *Biochimica et Biophysica Acta (BBA) -*
738 *Molecular Basis of Disease* 1812 (11): 1490–97.
739 <https://doi.org/10.1016/j.bbadis.2011.07.005>.
- 740 42. Xie, Rui, Susan Nguyen, Wallace L McKeehan, and Leyuan Liu. 2010. “Acetylated
741 Microtubules Are Required for Fusion of Autophagosomes with Lysosomes.” *BMC Cell*
742 *Biology* 11 (1): 89. <https://doi.org/10.1186/1471-2121-11-89>.
- 743 43. Yu, Jinyan, Mengshi Ma, Zhongsen Ma, and Jian Fu. 2016. “HDAC6 Inhibition Prevents
744 TNF- α -Induced Caspase 3 Activation in Lung Endothelial Cell and Maintains Cell-Cell
745 Junctions.” *Oncotarget* 7 (34): 54714–22. <https://doi.org/10.18632/oncotarget.10591>.
- 746 44. Zhang, Yu, SoHee Kwon, Teppei Yamaguchi, Fabien Cubizolles, Sophie Rousseaux,
747 Michaela Kneissel, Chun Cao, et al. 2008. “Mice Lacking Histone Deacetylase 6 Have
748 Hyperacetylated Tubulin but Are Viable and Develop Normally.” *Molecular and Cellular*
749 *Biology* 28 (5): 1688–1701. <https://doi.org/10.1128/MCB.01154-06>.
- 750

751

752

753 **Figure Legends**

754

755 **Figure 1: Regulation of HDAC6 activity by shear stress.** (A) Representative images and
756 analysis of expression of HDAC6 and phosphorylated-HDAC6 by immunofluorescence.
757 HUVECs exposed to high SS (HSS; 20 dyn/cm²) or low SS (LSS; 2 dyn/cm²) for 24 hours, were
758 labeled with HDAC6 (red), or phosphorylated-HDAC6 antibody (red), and the area/cell (μm²)
759 was analyzed (blue=DAPI). Quantification of total HDAC6 (B) and phosphorylated HDAC6 (C)
760 area in endothelial cells exposed to either high SS or low SS. Data represent means ± SEM of 6
761 independent experiments. (D) Analysis of HDAC6 activity in HUVECs exposed to high SS or
762 low SS for 24 hours. Data represent means ± SEM of 6 independent experiments, normalized to
763 low SS conditions. ns, not statistically different; **P* ≤ 0.05 (Wilcoxon test).

764

765

766 **Figure 2: Tubastatin-A treatment increases endothelial autophagy.** (A) Western blot analysis
767 of LC3 in HUVECs exposed to either high SS (HSS; 20 dyn/cm²) or low SS (LSS; 2 dyn/cm²)
768 and treated with either vehicle (DMSO: 0.1 μL/mL) or Tubastatin-A (TUBA; 3 μM) for 24
769 hours. (B) Quantification of the LC3-II/I (left) and LC3-II/GAPDH (right) ratios; data represent
770 means ± SEM of 6 independent experiments normalized to low SS + DMSO. (C) Representative
771 confocal microscopy images of HUVECs exposed to either high SS or low SS and treated with
772 either vehicle (DMSO: 0.1 μL/mL) or Tubastatin-A (TUBA; 3 μM) for 24 hours (blue: DAPI,
773 green: VE-cadherin, red: LC3). (D) Quantification of LC3 area per cell; data represent means ±
774 SEM of 6 independent experiments normalized to low SS + DMSO. **P* ≤ 0.05 (Wilcoxon test).

775

776 **Figure 3: Autophagic flux is restored in HUVECs exposed to low SS and treated with**
777 **Tubastatin-A.** (A) Representative confocal microscopy images of HUVECs infected with
778 lentiviruses carrying the tandem mRFP-GFP-LC3 plasmid and exposed to high SS (HSS; 20
779 dyn/cm²) or low SS (LSS; 2 dyn/cm²) for 24 hours, in the presence or absence of Tubastatin-A
780 (TUBA; 3 μM) or Rapamycin (RAPA; 1 μM). Autophagosomes and autolysosomes are denoted
781 by yellow and red signals, respectively. Scale bar: 25 μm. (B) Quantification of the number of
782 autophagy vacuoles per cell. Yellow bars correspond to the number of autophagosomes per cell
783 and red bars correspond to the number of autolysosomes per cell. HUVECs were exposed to
784 either high SS or low SS and treated with either vehicle (DMSO at 0.1 μL/mL), Rapamycin
785 (RAPA; 1μM) or Tubastatin-A (TUBA; 3 μM) for 24 hours. Quantification of the number of
786 autophagosomes (C) and autolysosomes (D) per cell. (E) Quantification of the number of

787 autophagy vacuoles per cell in HUVECs exposed to low SS and treated with Chloroquine
788 (CHLQ; 300 μ M) and either vehicle (DMSO at 0.1 μ L/mL) or Tubastatin-A (TUBA; 3 μ M) for
789 24 hours. Quantification of the number of autophagosomes (**F**) and autolysosomes (**G**) per cell in
790 HUVECs exposed to low SS and treated with Chloroquine (CHLQ; 300 μ M) and either vehicle
791 (DMSO at 0.1 μ L/mL) or Tubastatin-A (TUBA; 3 μ M) for 24 hours). Data represent means \pm
792 SEM of 6 independent experiments in which over 100 cells were analyzed per condition. ns, not
793 statistically different; * $P \leq 0.05$ (Wilcoxon test).

794

795 **Figure 4: Tubastatin-A has anti-inflammatory effect on endothelial cells exposed to low**
796 **shear stress. (A)** Western blot analysis of ICAM-1 in HUVECs exposed to high SS (HSS; 20
797 dyn/cm²) or low SS (LSS; 2 dyn/cm²) and treated with either vehicle (DMSO at 0.1 μ L/mL) or
798 Tubastatin-A (TUBA; 3 μ M) for 24 hours, in the presence or absence of TNF- α (1 ng/mL). (**B**)
799 Western blot analysis of VCAM-1 in HUVECs exposed to high SS (HSS; 20 dyn/cm²) or low SS
800 (LSS; 2 dyn/cm²) and treated with either vehicle (DMSO at 0.1 μ L/mL) or Tubastatin-A (TUBA;
801 3 μ M) for 24 hours, in the presence or absence of TNF- α (1 ng/mL). (**C**) Quantification of the
802 ICAM-1/GAPDH ratio; data represent means \pm SEM of 6 independent experiments normalized
803 to low SS + DMSO + TNF- α . (**D**) Quantification of the VCAM-1/GAPDH ratio; data represent
804 means \pm SEM of 6 independent experiments normalized to low SS + DMSO + TNF- α . (**E**)
805 ELISA analysis of MCP-1 levels released in the conditioned media of HUVECs exposed to high
806 SS (HSS; 20 dyn/cm²) or low SS (LSS; 2 dyn/cm²) and treated with either vehicle (DMSO at 0.1
807 μ L/mL) or Tubastatin-A (TUBA; 3 μ M) for 24 hours, in the presence or absence of TNF- α (1
808 ng/mL). Data represent means \pm SEM of 6 independent experiments. * $P \leq 0.05$ (Wilcoxon test).

809

810 **Figure 5: Knockdown of HDAC6 increases endothelial autophagy and reduces**
811 **inflammation. (A)** Western blots analysis of HDAC6, acetylated α -tubulin, LC3, ICAM-1 and
812 VCAM-1 expression in HUVECs transduced with either shControl (shCtl) or shHDAC6
813 lentiviruses and exposed to low SS (LSS; 2 dyn/cm²), in the presence or absence of TNF- α (1
814 ng/mL). Quantification of the HDAC6/GAPDH (**B**), acetylated α -tubulin/GAPDH (**C**), LC3-II/I
815 (**D**), ICAM-1/GAPDH (**E**) and VCAM-1/GAPDH (**F**) ratios; data represent means \pm SEM of 6
816 independent experiments normalized to shCtl. (**G**) ELISA analysis of MCP-1 levels released in
817 the conditioned media of HUVECs transduced with either shControl (shCtl) or shHDAC6
818 lentiviruses and exposed to low SS (LSS; 2 dyn/cm²), in the presence or absence of TNF- α (1
819 ng/mL). Data represent means \pm SEM of 6 independent experiments. * $P \leq 0.05$ (Wilcoxon test).

820

821 **Figure 6: Tubastatin-A is unable to reduce inflammation in ATG5-deficient endothelial**
822 **cells. (A)** Western blots analysis of ATG5, LC3, ICAM-1 and VCAM-1 expression in
823 endothelial cells transduced with either shControl (shCtl) or shATG5 lentiviruses, exposed to
824 low SS (LSS; 2 dyn/cm²), and treated with vehicle (DMSO at 0.1 μL/mL) or Tubastatin-A
825 (TUBA; 3 μM) in the presence of TNF-α (1 ng/mL). **(B)** Quantification of the LC3-II/I ratio.
826 Data represent means ± SEM of 6 independent experiments normalized to shCtl. Quantification
827 of Tubastatin-A induced changes in the expression of ICAM-1 **(C)** and VCAM-1 **(D)**; and
828 concentration of MCP-1 in the conditioned media of HUVECs **(E)**. Data represent means ± SEM
829 of 6 independent experiments. ns, not statistically different; **P* ≤ 0.05 (Wilcoxon test).

830

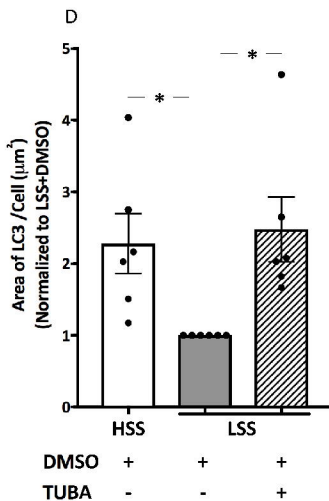
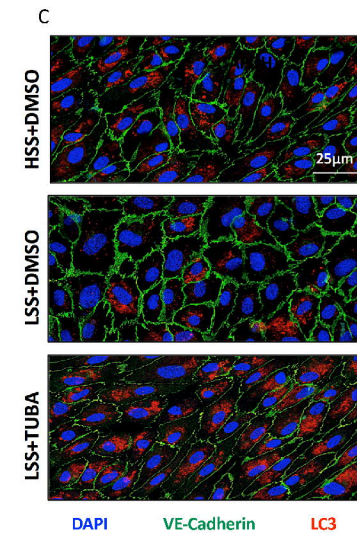
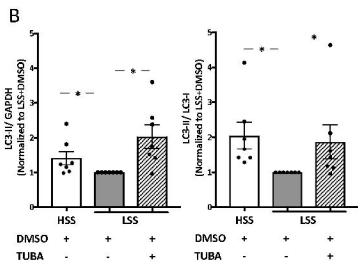
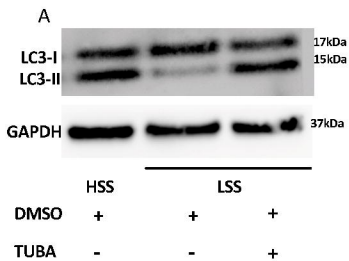
831 **Figure 7: HDAC6 knockout increases autophagic flux in atheroprone areas of the aorta.**
832 **(A)** LC3 *en face* staining of the aorta of *HDAC6*^{-/-}/*ApoE*^{-/-} mice and littermate controls
833 *HDAC6*^{+/+}/*ApoE*^{-/-}; n=3 per group; (red, LC3; blue, DAPI). **(B)** Data represent means ± SEM of
834 LC3 area per cell from 5 different photographic fields per mouse. **(C)** LC3 and LAMP2A *en face*
835 staining of the aorta of *HDAC6*^{-/-}/*ApoE*^{-/-} mice and littermate controls *HDAC6*^{+/+}/*ApoE*^{-/-}; n=3
836 per group; (red, LC3; green, LAMP2A; blue, DAPI). **(D)** Data represent means ± SEM of the
837 percentage of LC3 and LAMP2A colocalization from 5 different photographic fields per mouse.
838 **P* ≤ 0.05, ***P* ≤ 0.01, ****P* ≤ 0.001 (Two-way Anova and Sidak's post-test)

839

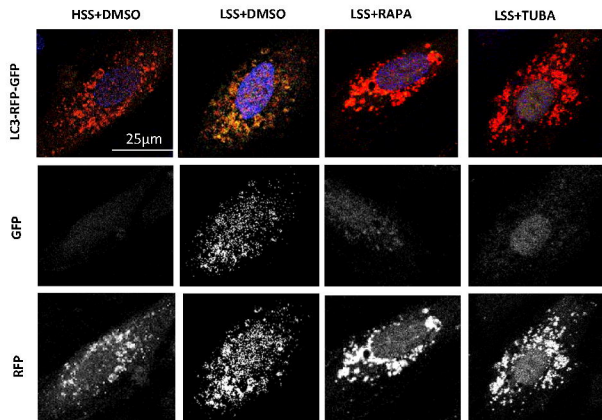
840 **Figure 8: HDAC6 knockout impairs plaque development in atheroprone areas of the aorta.**
841 Chimeric *HDAC6*^{-/-}/*ApoE*^{-/-} mice (n=13) and littermate controls *HDAC6*^{+/+}/*ApoE*^{-/-} (n=14),
842 transplanted with *HDAC6*^{+/+}/*ApoE*^{-/-} bone marrow were fed with a high fat diet for 10 weeks.
843 Representative images **(A)** and quantification **(B)** of *en face* Oil Red-O staining of
844 atherosclerotic lesions in the mice aorta. Data represent means ± SEM. ns, not statistically
845 different; ****P* ≤ 0.001 (Mann-Whitney test).

846

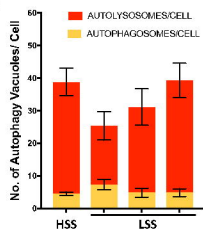
847



A

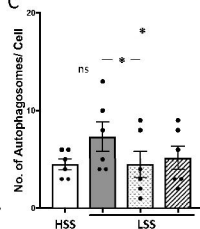


B



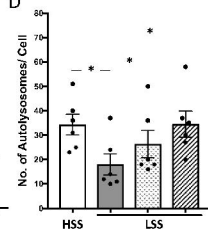
	DMSO	RAPA	TUBA
HSS	+	-	-
LSS	+	+	-
LSS	+	-	+
LSS	+	+	+

C



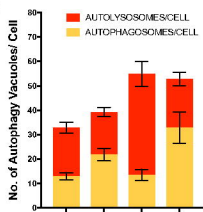
	DMSO	RAPA	TUBA
HSS	+	-	-
LSS	+	+	-
LSS	+	-	+
LSS	+	+	+

D



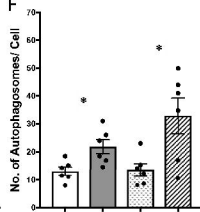
	DMSO	RAPA	TUBA
HSS	+	-	-
LSS	+	+	-
LSS	+	-	+
LSS	+	+	+

E



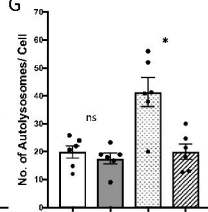
	LSS	DMSO	CHLQ	TUBA
LSS	+	+	-	-
LSS	+	+	+	-
LSS	+	+	-	+
LSS	+	+	+	+

F



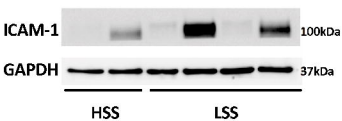
	LSS	DMSO	CHLQ	TUBA
LSS	+	+	-	-
LSS	+	+	+	-
LSS	+	+	-	+
LSS	+	+	+	+

G



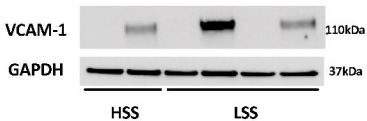
	LSS	DMSO	CHLQ	TUBA
LSS	+	+	-	-
LSS	+	+	+	-
LSS	+	+	-	+
LSS	+	+	+	+

A



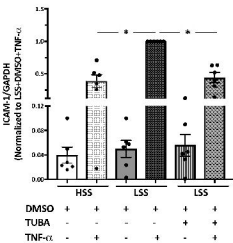
	HSS			LSS		
DMSO	+	+	+	+	+	+
TUBA	-	-	-	+	+	+
TNF- α	-	+	-	+	-	+

B

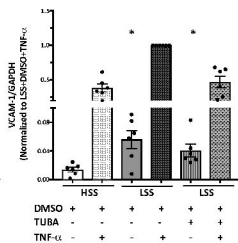


	HSS			LSS		
DMSO	+	+	+	+	+	+
TUBA	-	-	-	+	+	+
TNF- α	-	+	-	+	-	+

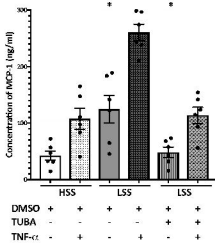
C

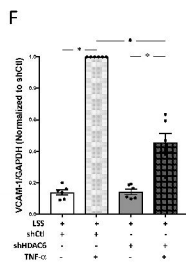
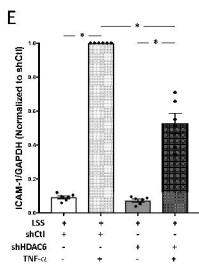
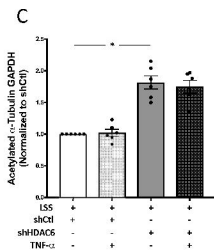
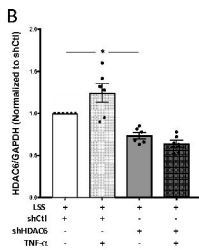
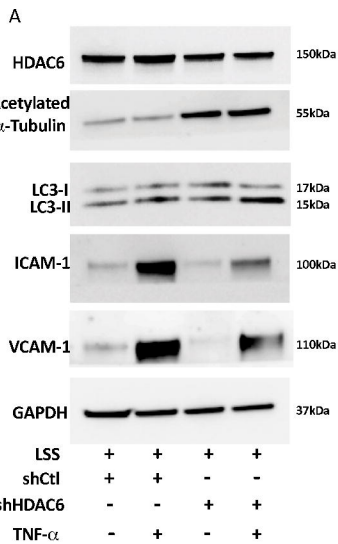


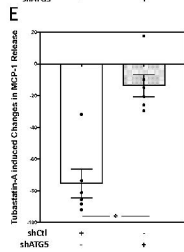
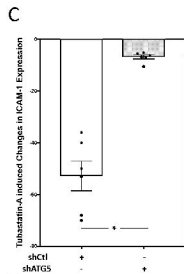
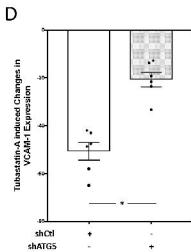
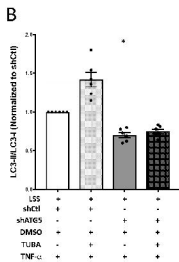
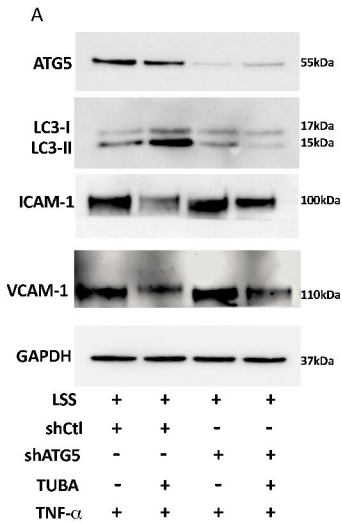
D

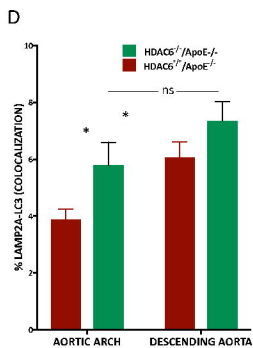
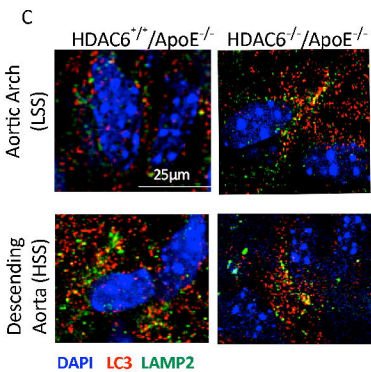
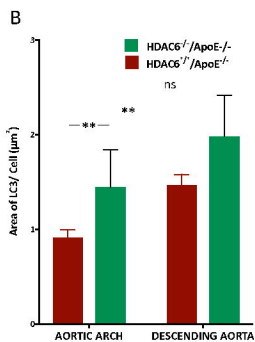
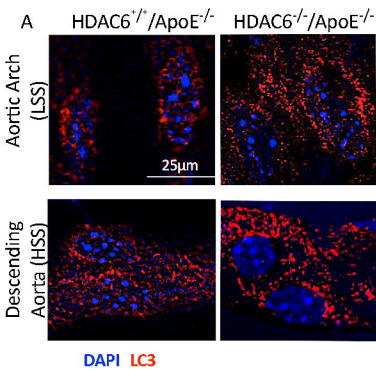


E









A



B

